Electronic Supplementary Material (ESI) for Journal of Materials Chemistry A.

Free-standing Metal-organic Frameworks on Electrospun Core-shell Graphene Nanofibers for Flexible Hybrid Supercapacitors

Nissar Hussain[a], Zahir Abbas[a], Kallayi Nabeela [a], Shaikh M. Mobin*[, a, b,]

[a] Department of Chemistry, Indian Institute of Technology Indore, Simrol, Khandwa Road, Indore 453552, India.

[b] Center for Advance Electronics (CAE), Indian Institute of Technology Indore, Simrol, Khandwa Road, Indore 453552, India.

*E-mail: xray@iiti.ac.in (Shaikh M. Mobin)

Tel: +91 731 6603 336

Table of Contents

Material Characterizations

All the reagents and solvents were purchased from a commercial source without any further purification. Cu K (0.154 nm) monochromatic radiation was employed with a Rigaku Smart Lab X-ray diffractometer for the Powder X-ray Diffraction (PXRD) investigation. The morphology of samples was captured on a Zeiss Supra55 field-emission scanning electron microscope (FE-SEM). pictures were taken (FESEM) and 200 KV (Tecnai G2 F 30) transmission electron microscope (TEM). Brunauer-Emmett-Teller (BET) surface area of the composite and its Barrett-Joyner-Halenda (BJH) pore size distribution were found out on an Autosorb iQ, (Quantachrome Instruments, version 1.11). using N_2 flow, X-ray photoelectron spectroscopy (XPS) was performed on an XPS spectrometer (PHI 5000 VersaProbe III spectrophotometer (ULVAC-PHI INC), using Al Kα as the X-ray source. The tensile strength of the samples was used as a parameter to measure the mechanical strength of the GNF and c-MOF@GNF. A UTM AGX-V (Shimadzu) was used to record the tensile strength. The size of the samples was 40 mm × 10 mm used for the tests which were all performed at ambient temperature and humidity.

Electrochemical measurement in a three-electrode system

The as-prepared c-MOF@GNF freestanding electrode was carefully cut into 1 × 1 cm^2 (a mass loading of 3 mg was used as a working electrode with Ag/AgCl as a reference electrode, and platinum wire as the counter electrode in three electrodes set up. To determine the electrochemical performance, cyclic voltammetry (CV), galvanostatic charge-discharge (GCD) curve measurements, and electrochemical impedance spectroscopy (EIS) were carried out on Autolab workstation using a 2M KOH aqueous solution as an electrolyte. The efficiency evaluation was determined by the following equations summarised above. The electrochemical study of control samples i.e., pristine c-MOF is studied by drop casting MOF on Ni foam (NF) as a working electrode (dispersion in ethanol achieved a mass loading is around 2 mg).

Device fabrications

The two-electrode system was fabricated using carbon cloth as the current collector. As for the electrolytes, PVA–KOH was applied to the electrodes. PVA (1 g) was added to H_2O (10 mL) at 90 °C to produce a transparent solution. Subsequently, 3.0 g of KOH in 10 mL of water was added with full agitation until the PVA aqueous solution cooled to room temperature. Finally, PVA–KOH gel was coated on the electrode, which was solidified at room temperature. Finally, the assembly of the solid-state supercapacitor demonstrated that the positive electrode and

negative electrode were completely separated by cellulose paper and fixed for further use to record the efficiency of the devices.

Electrochemical Calculations

The specific capacitance (C_S) of electrodes can be calculated from the galvanostatic charge/discharge curves using eqn. 1:

$$C = \frac{I\Delta t}{m\Delta V} \quad (1)$$

where I/m, Δt, and ΔV represent the current density, constant discharge time, and potential window, respectively.

The specific capacity (C g^{-1}) of the electrode was estimated using the eqn. 2:

$$C = \frac{I}{m}\Delta t \quad (2)$$

where I/m and Δt depicts the current density and discharge time, respectively.

In the hybrid devices, the charge balance between the two electrodes needs to follow the relationship $q^+ = q^-$ and the optimal mass ratio between the positive electrode and negative electrode can be obtained according to eqn. 3:

$$\frac{m^+}{m^-} = \frac{C^- \times \Delta V^-}{C^+ \times \Delta V^+} \quad (3)$$

where m^+, ΔV^+ and C^+ are the mass, potential, and specific capacity of the positive electrode respectively, and m^-, ΔV^- and C^- are the mass, potential, and specific capacity of the negative electrode, respectively. The optimized mass ratio of the c-MOF@GNF positive electrode and GNF negative electrode used in the fabrication of the hybrid device as calculated using eqn. 3 was 2 : 1.

The energy density (E) of the device was evaluated according to Eqn. 3:

$$E = \frac{C}{2 \times 3.6} \times \Delta V^2 \quad (4)$$

Where C is the specific capacitance, ΔV is the working potential window.

The power density (P) of the device is calculated according to eqn. 4:

$$P = \frac{E}{\Delta t} \times 3600 \quad (5)$$

Where E depicts the energy density, t is the discharging time (h)

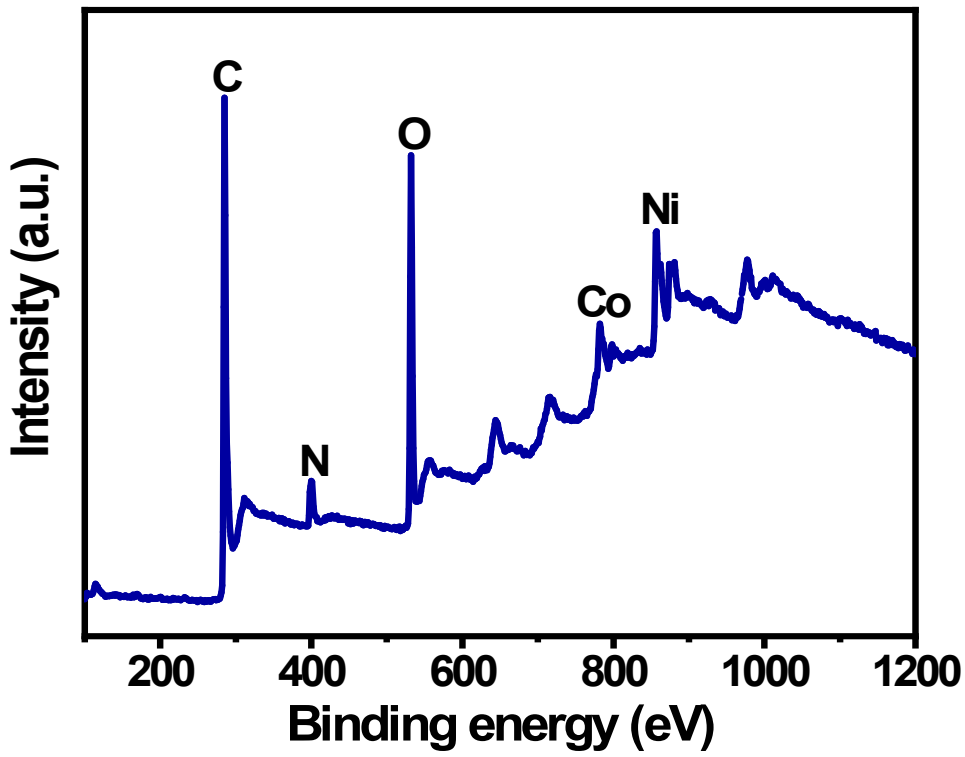

Fig S1: XPS survey scan of c-MOF@GNF.

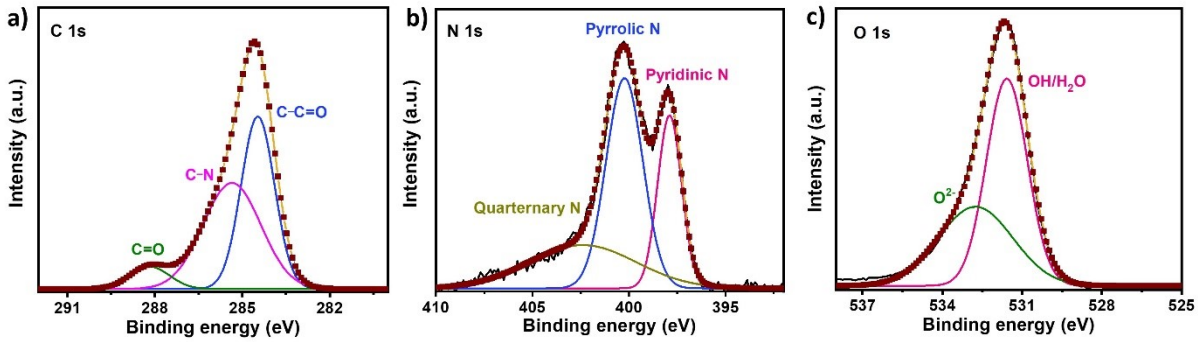

Fig S2. The high-resolution XPS spectra of c-MOF@GNF a) Carbon (C 1s), b) Nitrogen (N 1s), and c) Oxygen (O 1s)

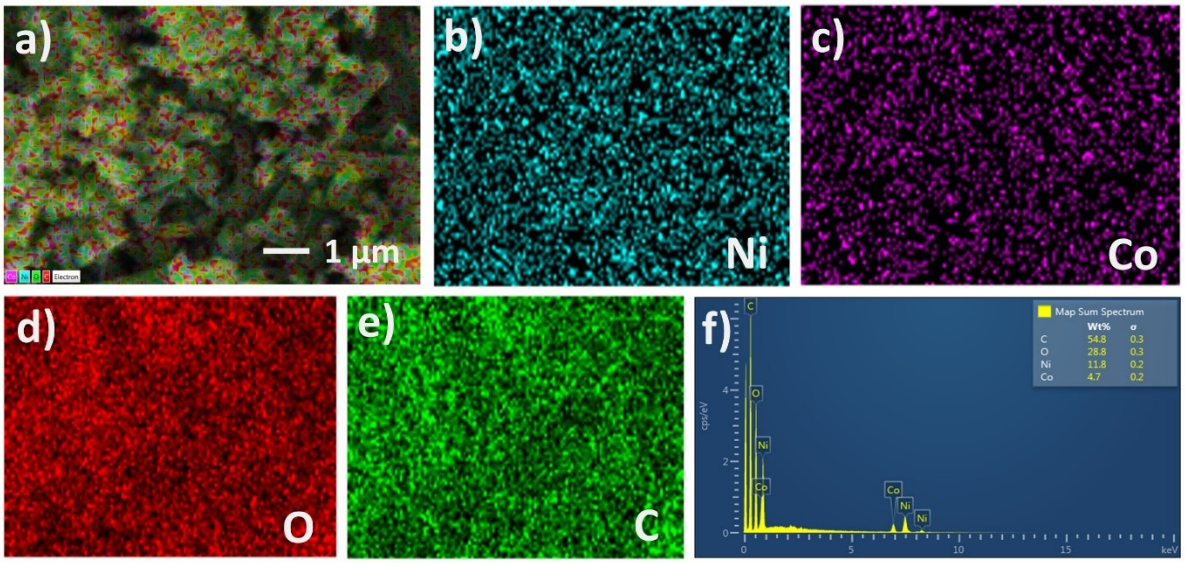

Fig S3. EDX map of c-MOF a) composite Ni, Co, O, and C, b) Nickel (Ni), c) Cobalt (Co), d) Oxygen (O), e) Carbon (C). f) EDX spectrum with percentage count.

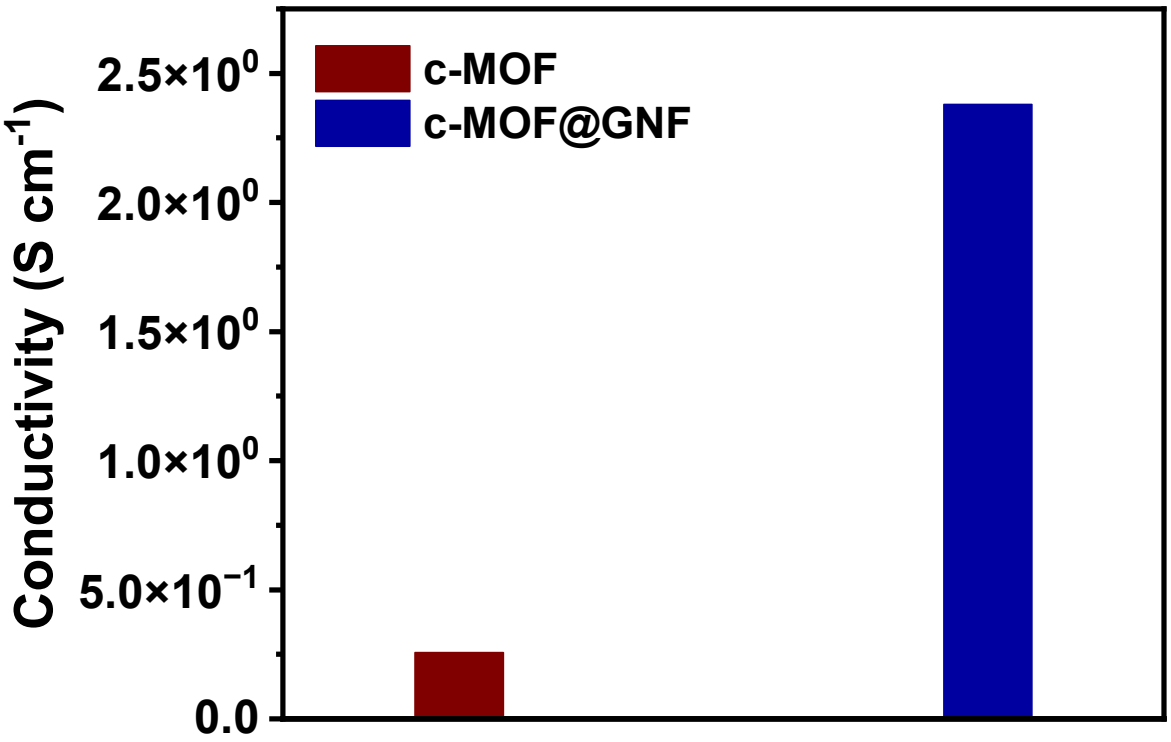

Fig S4. Electrical conductivity of c-MOF and c-MOF@GNF.

Table S1. Comparison of electrical conductivity with other MOF-based composites.

MOF Composites	**Electrical Conductivity S cm $^{-1}$**	**References**
NU-901@C60	1×10^{-3}	1
cc-HBC-120-Cu	3.31 S cm^{-1}	2
TCNQ@Cu_3BTC_2	1.5×10^{-4} S cm^{-1}	3
Zr-bzpdc-MOF@PEDOT	1×10^{-2}	4
MIL-101@PEDOT	1.1×10^{-3}	5
c-MOF@GNF	**23.8×10^{-1}**	**This work**

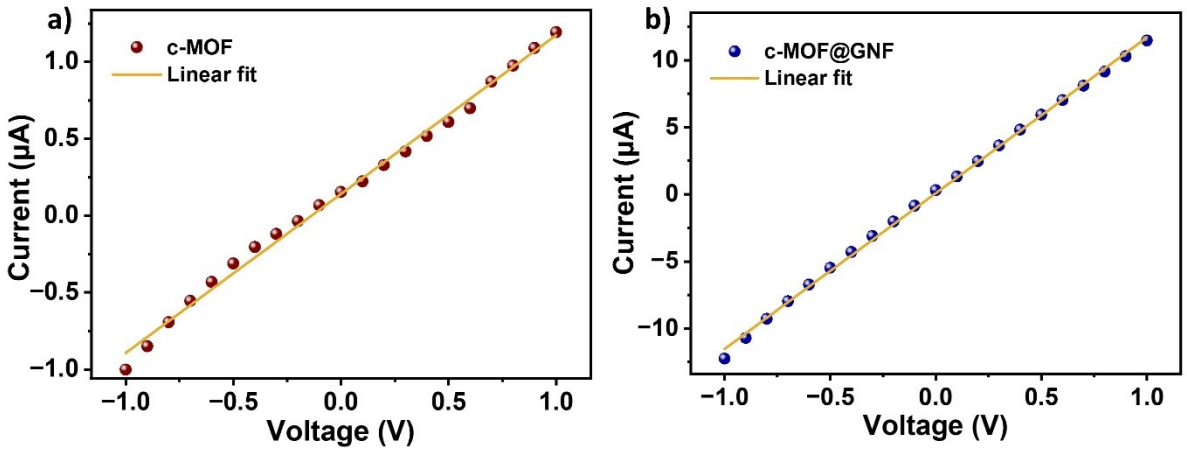

Fig S5. Electrical conductivity measurements: Current (I) *vs* voltage (V) plot for a) c-MOF and b) c-MOF@GNF

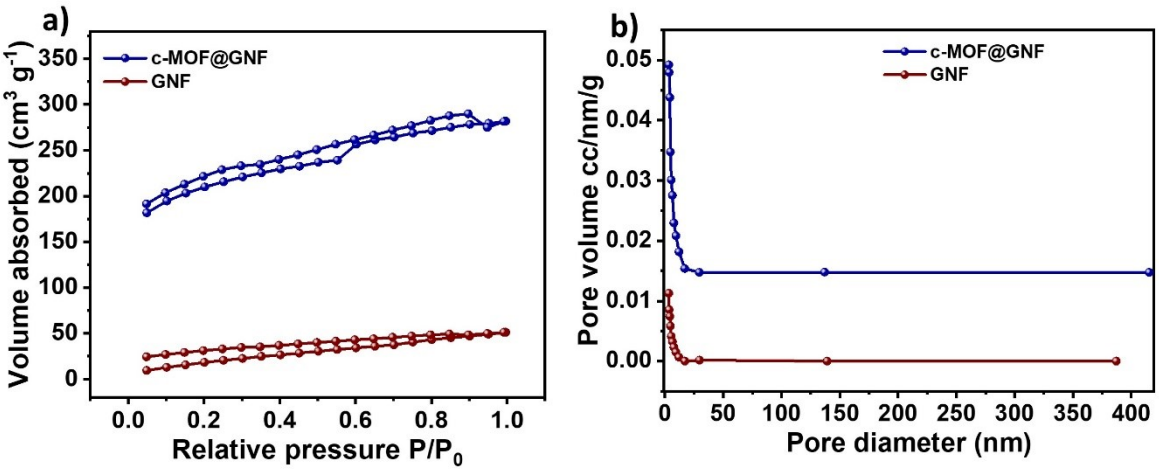

Fig S6. a) N_2 adsorption and desorption b) BJH pore size distribution of c-MOF@GNF and GNF respectively.

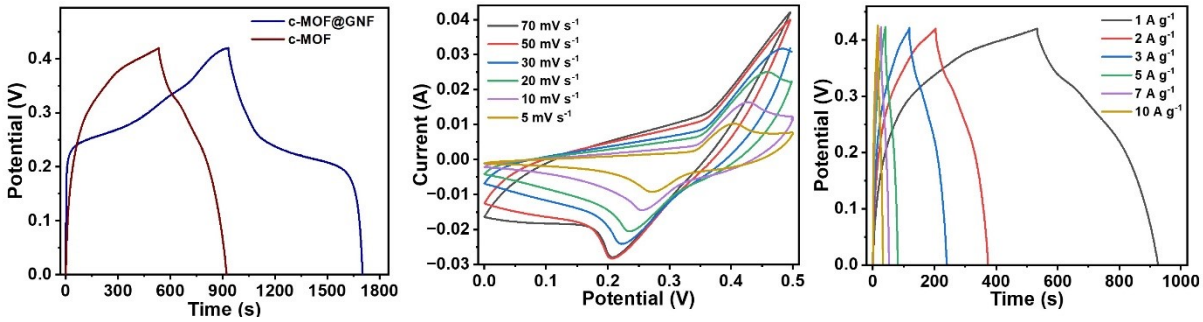

Fig S7. a) GCD comparison of c-MOF and c-MOF@GNF at 1A g^{-1}. Electrochemical performance of c-MOF b) CV curves at different scan rates from 5 to 70 mV s^{-1} c) GCD curves at different current densities from 1 to 10 A g^{-1}.

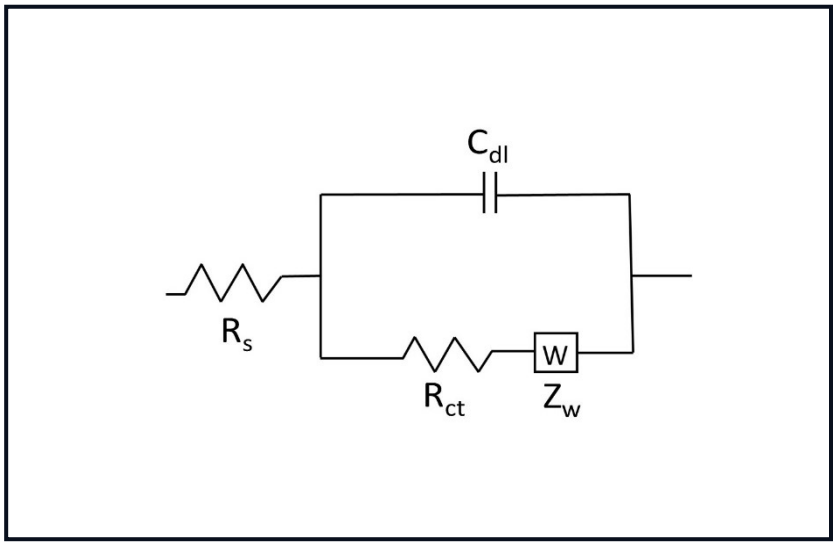

Fig S8. EIS circuit fit.

Table S2: Circuit parameters obtained after fitting the EIS data to the used equivalent circuit.

Resistance Parameters	**c-MOF@GNF**	**c-MOF**
$\mathbf{R_{ct}}$	3.23 Ω	5.60 Ω
$\mathbf{R_s}$	1.35 Ω	3.35 Ω
$\mathbf{C_{dl}}$	272 μF	460 μF
$\mathbf{R_w}$	33.0 $mMhos^{1/2}$	56.0 $mMhos^{1/2}$

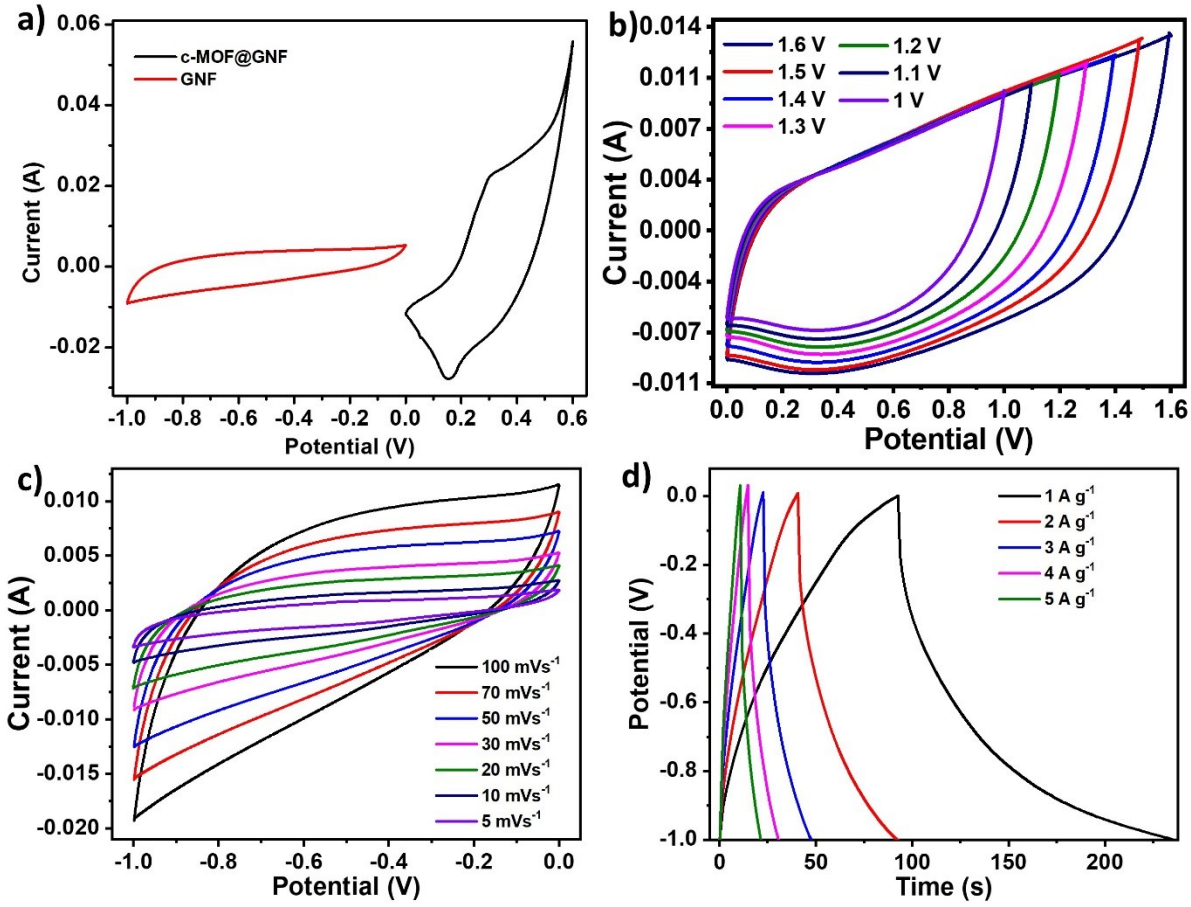

Fig S9. a) CV curves of c-MOF@GNF and GNF at a scan rate of 50 mv s^{-1} in a three-electrode system.CV curves of b) CV curve c-MOF@GNF//GNF at different potential windows. Electrochemical studies of GNF c) CV curves at different scan rates and d) GCD curves at different current densities.

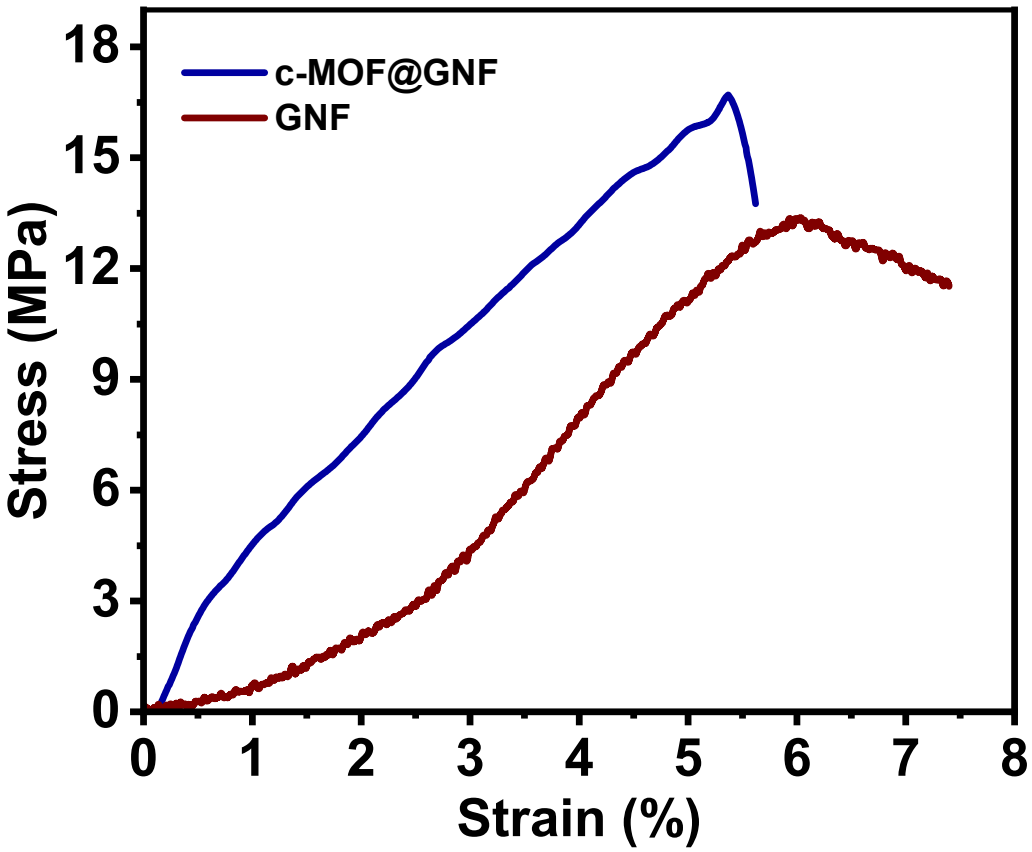

Fig S10. Stress-strain curves of GNF and c-MOF@GNF.

Table S3. Comparison of as-synthesized material with previous reports

S. No.	Material	Specific capacitance ($F\ g^{-1}$)	Rate ($A\ g^{-1}$)	Electrolyte	Capacitive retention	Ref.
1	MX-5@PCNF	527 $F\ g^{-1}$	1 Ag^{-1}	3 M KOH	96.4% capacitance retention after 10 000 cycles	6
2	rOHNM-AGs	1644 $F\ g^{-1}$	1 Ag^{-1}	6 M KOH	87.8% after 10,000 cycles	7
3	PPy@NiCo-CAT	572.2 $F\ g^{-1}$	1 $A\ g^{-1}$	2 M KOH	54.7% after 5000 cycles	8
4	Redox active NiFc-MOF@CNF	1150 F^{-1}	1 $A\ g^{-1}$	3 M KOH	82.2% after 25000 cycles	9
5	BP/ZIF 67	1347 $F\ g^{-1}$	0.5 $A\ g^{-1}$		90.4% after 5,000 cycles	10
7	PPNF@Co-Ni MOF	1092.2 $F\ g^{-1}$	1 $A\ g^{-1}$	3 M KOH	____	11
8	Ni-MOF/CNTs	1765 $F\ g^{-1}$	0.5 $A\ g^{-1}$	6 M KOH	____	12
9	CNF@Ni-CAT	502.95 g^{-1}	0.5 $A\ g^{-1}$	2 M KOH	73% after 5,000 cycles	13
10	**c-MOF@GNF**	**1820 $F\ g^{-1}$**	**1 $A\ g^{-1}$**	**2 M KOH**	**91.6% after 14,000 cycles**	**This work**

References

1 S. Goswami, D. Ray, K. Otake, C.-W. Kung, S. J. Garibay, T. Islamoglu, A. Atilgan, Y. Cui, C. J. Cramer, O. K. Farha and J. T. Hupp, *Chem. Sci.*, 2018, **9**, 4477–4482.

2 G. Xing, J. Liu, Y. Zhou, S. Fu, J.-J. Zheng, X. Su, X. Gao, O. Terasaki, M. Bonn, H. I. Wang and L. Chen, *J. Am. Chem. Soc.*, 2023, **145**, 8979–8987.

3 C. Schneider, D. Ukaj, R. Koerver, A. A. Talin, G. Kieslich, S. P. Pujari, H. Zuilhof, J. Janek, M. D. Allendorf and R. A. Fischer, *Chem. Sci.*, 2018, **9**, 7405–7412.

4 A. Mohmeyer, A. Schaate, B. Hoppe, H. A. Schulze, T. Heinemeyer and P. Behrens, *Chem. Commun.*, 2019, **55**, 3367–3370.

5 B. Le Ouay, M. Boudot, T. Kitao, T. Yanagida, S. Kitagawa and T. Uemura, *J. Am. Chem. Soc.*, 2016, **138**, 10088–10091.

6 I. Pathak, D. Acharya, K. Chhetri, P. C. Lohani, S. Subedi, A. Muthurasu, T. Kim, T. H. Ko, B. Dahal and H. Y. Kim, *J. Mater. Chem. A*, 2023, **11**, 5001–5014.

7 H. Zong, A. Zhang, J. Dong, Y. He, H. Fu, H. Guo, F. Liu, J. Xu and J. Liu, *Chemical Engineering Journal*, 2023, **475**, 146088.

8 K. Chen, S. Zhao, J. Sun, J. Zhou, Y. Wang, K. Tao, X. Xiao and L. Han, *ACS Appl. Energy Mater.*, 2021, **4**, 9534–9541.

9 Z. Abbas, N. Hussain, S. Kumar and S. M. Mobin, *Nanoscale*, 2024, **16**, 868–878.

10 T. Wu, Z. Ma, Y. He, X. Wu, B. Tang, Z. Yu, G. Wu, S. Chen and N. Bao, *Angewandte Chemie International Edition*, 2021, **60**, 10366–10374.

11 D. Tian, N. Song, M. Zhong, X. Lu and C. Wang, *ACS Appl. Mater. Interfaces*, 2020, **12**, 1280–1291.

12 P. Wen, P. Gong, J. Sun, J. Wang and S. Yang, *J. Mater. Chem. A*, 2015, **3**, 13874–13883.

13 S. Zhao, H. Wu, Y. Li, Q. Li, J. Zhou, X. Yu, H. Chen, K. Tao and L. Han, *Inorg. Chem. Front.*, 2019, **6**, 1824–1830.